AIMS Mathematics, 11(7): 21781–21798.
DOI: 10.3934/math.2026881
Received: 07 May 2026
Revised: 25 June 2026
Accepted: 13 July 2026
Published: 22 July 2026

https://www.aimspress.com/journal/Math

Research article

Numerical solution of nonlinear reaction-diffusion systems by a novel Taylor series method versus the Galerkin finite element method

Badran Jasim Salim*

Department of Mathematics, College of Basic Education, University of Mosul, Iraq

* **Correspondence:** Email: dr.badranjasim@uomosul.edu.iq.

Abstract: This study presents a comprehensive analysis and comparison of two numerical approaches for handling the nonlinear Lotka-Volterra interaction and diffusion system: the novel Taylor series method (NTSM) and the Galerkin finite element method (GFEM). We develop a semi-analytical NTSM method by iteratively obtaining coefficients from the governing partial differential equations and initial and boundary conditions to construct high-order Taylor series in space and time. The method is validated by comparison with an exact analytic solution, demonstrating high accuracy at the real-solution level (achieving errors below machine precision (approximately 10^{-16}) in the tested scenarios) and rapid convergence, attributed to the analytic nature of the underlying solution. Furthermore, the use of linear (hierarchical) basis functions and Galerkin weighting with GFEM provides robust and physically acceptable approximations that rapidly achieve the stable equilibrium state of the system. Using Maple 18 and MATLAB, numerical tests indicate that the GFEM is robust and suitable for complex geometries and extended dynamics; however, the NTSM method significantly outperforms it in terms of accuracy and convergence speed for smooth and well-defined boundary problems in straightforward analytical problems. The results obtained show the accuracy and efficiency of NTSM in solving analytical and numerical problems, while GFEM is characterized by its strength in complex domains. Theoretical convergence analysis confirms an $O(h^2)$ order convergence for GFEM and an exponential convergence for NTSM in the smooth test cases examined in this study, thus supporting the numerical results.

Keywords: Galerkin finite element method; Lotka-Volterra system; nonlinear partial differential equation system; novel Taylor series method
Mathematics Subject Classification: 35K57, 65M60, 65Z05, 92D25

1. Introduction

The Galerkin finite element method (GFEM) is a fundamental numerical method used to solve complex problems in various fields such as engineering and mathematical physics. Its main advantage lies in its ability to solve nonlinear problems as well as analyze complex geometric structures, which are difficult to solve analytically [1]. In contrast, the Taylor series is an effective, applicable, simple, and easy-to-use tool. However, when high-precision results are needed, their usefulness is limited due to their slow convergence rate [2]. The Lotka-Volterra interaction and diffusion model remains an important area of study and research utilizing analytical and numerical techniques, with a focus on investigating the convergence and stability of this system.Many researchers have conducted comprehensive studies in understanding traveling waves and propagation and interaction issues using numerous numerical and analytical methods in order to provide accurate and specific solutions for these systems. Costin et al. have verified Cauchy's problems for generalized telegraph equations and have approached the realm of nonlinear differential equations [3]. Tsga [4] provided a numerical solution to the diffusion and reaction equations represented by the three-dimensional thermal conductivity equation. Salim and Merie used the exponential function to find the analytical solution to the Lotka-Volterra system [5]. Salim solved a three-dimensional system numerically using the finite volume method and identified the stability points of this system [6]. Some classical works studied the basics using various analytical and numerical methods to solve the equations of reaction and diffusion [7, 8]. Salim [9] Microwave-based methods have been explored for solving nonlinear systems, including sine-cosine waves, a numerical technique for solving differential and integral equations. Jassim [10] Runge-Kota charts for higher ranks were developed and good results were obtained. Some numerical methods, such as the finite difference method, have been used to solve various models of reaction and diffusion equations and have obtained approximate estimates of finite and fractional differences [11, 12]. Other work has contributed to the development of some problems using Galerkin's discrete method and traveling wave analysis [13–15]. The nonlinear Lotka-Volterra system has been studied using several numerical methods, such as the finite element method and the Laplace-Adomian method, with acceptable results obtained [16–18]. Other modern applications include studying the stability of linear and nonlinear systems, stochastic control, and series expansions using generalized alpha difference factors [19, 20]. Recent developments include combined alternating direction implicit schemes of higher-order nonlinear partial differential equations with weakly singular multiple nuclei [21], combined alternating direction implicit schemes of differences for fractional integral differential equations [22], and spatiotemporal bilattice methods for nonlocal transport models [23]. These typically rely on finite differences or finite elements on structured networks. The proposed novel Taylor series method (NTSM) method is characterized by being a semi-analytical approach that generates Taylor series directly from partial differential equations, which eliminates segmentation errors and achieves highly efficient spectral accuracy for smooth solutions. However, the NTSM method shows maximum effectiveness when applied specifically to analytical systems, while the methods mentioned above excel in handling a wider range of problems involving single cores or non-local interactions, due to the robustness of network-based schemes in these cases. Despite these developments, a systematic comparative analysis between Taylor's methods and established finite element approaches, and their application to Lotka-Volterra interaction and diffusion systems, has not been adequately studied. In this paper, we investigate the

numerical solution of a Lotka-Volterra system using the GFEM and compare these results with those obtained using the NTSM; comparing the two methods with a precise analytical solution targets elements of accuracy, convergence speed, and computational efficiency, giving researchers a clear practical view of the choice between available solutions in the field of nonlinear environmental modeling. Despite the classical nature of the Taylor series, the depth of this work lies in the extension of its developed method to include a systematic comparison with the finite element method of the Lotka-Volterra model, while providing quantitative proof of its exponential convergence to smooth problems, and demonstrating its numerical accuracy in solving these complex systems.

2. Mathematical model

In this study, we use the Lotka-Volterra nonlinear interaction and diffusion system to apply the two numerical methods to determine the accuracy and efficiency of each method, and also to demonstrate the stability of this system, represented in the following:

$$\begin{aligned} \frac{\partial p}{\partial t} &= \phi_1 \Delta p + p(k_1(x) - p - q), \\ \frac{\partial q}{\partial t} &= \phi_2 \Delta q + q(k_2(x) - p - q), \end{aligned} \tag{2.1}$$

where, for the one-dimensional case considered in this study, $\Delta = \frac{\partial^2}{\partial x^2}$ denotes the standard Laplace operator (the extension to two-dimensional problems is straightforward). ϕ_1 and ϕ_2 represent the diffusion coefficients for the two species, respectively. This formula constitutes the Lotka-Volterra model [24], with the following initial conditions:

$$\begin{aligned} p(x,0) &= p_0(x), \qquad x \in [0, L], \\ q(x,0) &= q_0(x), \qquad x \in [0, L]. \end{aligned} \tag{2.2}$$

Where p_0 and q_0 are constant initial solutions of the Lotka-Volterra system and Neumann boundary conditions:

$$\frac{\partial p}{\partial x} = \frac{\partial q}{\partial x} = \begin{cases} e^t, & \text{at } x = 0, \\ e^{L+t}, & \text{at } x = L. \end{cases} \tag{2.3}$$

These boundary conditions are consistent with the exact solution, since for

$$p_{\text{exact}}(x,t) = e^{(x+t)/10} + \phi_1 \quad \text{and} \quad q_{\text{exact}}(x,t) = e^{(x+t)/10},$$

the spatial derivatives are

$$\partial p/\partial x = \partial q/\partial x = e^{(x+t)/10},$$

which matches the prescribed Neumann conditions at $x = 0$ (e^t) and $x = L$ (e^{L+t}).

3. Numerical method

In this section, the Lotka-Volterra system for nonlinear interaction diffusion (2.1) is solved using NTSM and GFEM, and compared with a precise analytical solution to evaluate accuracy, convergence behavior, and computational efficiency.

3.1. GFEM

GFEM is employed to obtain a numerical approximate of the nonlinear reaction-diffusion system (2.1). The exact population densities, p(x,t) and q(x,t) are approximated by trial function expressed as:

$$\begin{aligned} p_h(x,t) &= \sum_{i=1}^{N} P_i(t)\,\varphi_i(x), \\ q_h(x,t) &= \sum_{i=1}^{N} Q_i(t)\,\varphi_i/10(x), \end{aligned} \tag{3.1}$$

where $\varphi_i(x)$ are standard piecewise-linear basis functions defined over a uniform spatial mesh, and $P_i(t)$,$Q_i(t)$ represent the unknown time-dependent nodal coefficients. Substituting these approximations into the governing equation yield the residual:

$$R_p = \frac{\partial p_h}{\partial t} - \phi_1 \frac{\partial^2 p_h}{\partial x^2} - p_h(k_1(x) - p_h - q_h),$$

and similarly for R_q from the second equation. The expression for R_p is written here in its strong (differential) form for notational convenience. In the actual application of finite elements, the weak formulation is used, where the diffusion term is integrated by parts transferring the second derivative to the test function, this eliminating the need to calculate the second derivatives for the piecewise linear approximation, p_h. According to the method of weighted residuals, Galerkin's criterion requires that each residual, when weighted by the corresponding basis function, vanishes over the spatial domain [0, L]:

$$\begin{aligned} &\int_0^L R_p(x,t)\,\varphi_j(x)\,dx = 0, \\ &\int_0^L R_q(x,t)\,\varphi_j(x)\,dx = 0, \end{aligned} \qquad j = 1,\ldots,N,$$

where R_p and R_q denote the residuals associated with the first and second equations of system (2.1), respectively. This leads to a semi-discrete system of coupled nonlinear ordinary differential equations in time. Applying an implicit Euler temporal discretization, the unknown nodal values at the time level t^{m+1} are obtained by solving the resulting algebraic system. The contributions from each element are assembled into global matrices of the form

$$A^{(e)}\,U^{(m+1)} = b^{(e)},$$

where $U^{(m+1)}$ contains the complex unknowns, and $b^{(e)}$ contains the known values and sources from the previous step. $[x_i, x_j]$ defined as

$$\begin{aligned} N_i^{(e)}(x) &= \frac{x_j - x}{L_e}, \\ N_j^{(e)}(x) &= \frac{x - x_i}{L_e}, \end{aligned}$$

where $L_e = x_j - x_i$ is the element length. The derivation of these functions is as follows:

$$\begin{aligned} \frac{dp_h^{(e)}}{dx} &= \frac{dN_i}{dx} P_i + \frac{dN_j}{dx} P_j, \\ \frac{dq_h^{(e)}}{dx} &= \frac{dN_i}{dx} Q_i + \frac{dN_j}{dx} Q_j. \end{aligned} \tag{3.2}$$

The remaining values are calculated by integrating each element using the rules of squaring, and by using the Gaussian elimination method, we solve the Lotka-Volterra system, thus ensuring a stable and convergent numerical solution [25]. To further optimize the numerical solution, the GFEM is used. The integrals are then calculated using iterative methods such as Legendre's rule and the Newton-Raphson method, with the system being solved for $\epsilon = 10^{-6}$ to ensure repeatability. The computational domain Ω is partitioned such that

$$\Omega = \bigcup_{e=1}^{N_e} \Omega_e.$$

To approximate unknown fields, linear Lagrange functions are used to ensure the continuity of solutions to elements within the field.

3.1.1. Residuals and weighting function

Consider an element with nodes i and j, where the nodal unknowns at time space $m + 1$ are to be determined. A set of weighting functions $W_i^{(e)}$ and $W_j^{(e)}$ is defined over the element domain. The element residuals associated with nodes i and j for the first equation of system (2.1) are denoted by $R_i^{(e)}$ and $R_j^{(e)}$ respectively, and are given by:

$$\begin{aligned} R_i^{(e)} &= \int_{L^{(e)}} W_i^{(e)} \, r^{(e)} \, dx, \\ R_j^{(e)} &= \int_{L^{(e)}} W_j^{(e)} \, r^{(e)} \, dx. \end{aligned} \tag{3.3}$$

Here, $r^{(e)}$ represents the residual of the first equation evaluated over the element. Similarly, for the second equation of system (2.1), the element residuals at nodes i and j are denoted by $O_i^{(e)}$ and $O_j^{(e)}$, respectively, and are defined as:

$$\begin{aligned} O_i^{(e)} &= \int_{L^{(e)}} W_i^{(e)} \, o^{(e)} \, dx, \\ O_j^{(e)} &= \int_{L^{(e)}} W_j^{(e)} \, o^{(e)} \, dx. \end{aligned} \tag{3.4}$$

Where $o^{(e)}$ is the residual of the second equation over the same element. The Galerkin method is employed in this spatiotemporal finite element formulation. After substituting the approximations for p_h and q_h into the governing equations, the residual at node i within element (e) for the first equation becomes:

$$R_i^{(e)} = \int_{L^{(e)}} \Big[\frac{\partial p_h}{\partial t} - \phi_1 \frac{\partial^2 p_h}{\partial x^2} - p_h \left(k_1(x) - p_h - q_h \right) \Big] W_i^{(e)} \, dx. \tag{3.5}$$

For the second equation, the residual at node i is

$$O_i^{(e)} = \int_{L^{(e)}} \Big[\frac{\partial q_h}{\partial t} - \phi_2 \frac{\partial^2 q_h}{\partial x^2} - q_h \left(k_2(x) - p_h - q_h \right) \Big] W_i^{(e)} \, dx. \tag{3.6}$$

Analogous expressions hold for the residuals at node j. These integral equations form the basis for constructing the discrete system of equations to be solved at each time step.

3.1.2. Element matrices and column

The element residual equations are expressed in matrix form for efficient assembly into the global system:

$$R^{(e)} = A^{(e)}\, U^{(m+1)} - b^{(e)}, \tag{3.7}$$

where $R^{(e)}$ is the element residual vector containing $R_i^{(e)}$, $R_j^{(e)}$, $O_i^{(e)}$, and $O_j^{(e)}$, $A^{(e)}$ is the element matrix containing coefficients of the unknown nodal values at time step $m+1$, $b^{(e)}$ is the element column vector containing known terms from the previous time step m, and $U^{(m+1)}$ is the vector of unknown nodal values at time step $m+1$.

To fully address the structural non-linearity within the reaction terms without resorting to computational Newton-Raphson iterations, an explicit (lagged-in-time) Picard-type linearization strategy is applied. The unknown solution functions p_h and q_h present within the algebraic reaction components are evaluated lagged-in-time using the known nodal coefficients from the previous time level t_m (denoted as $p_h^{(m)}$ and $q_h^{(m)}$). This effectively maps the non-linear coupling directly onto the linear algebraic assembly system at the current time level t_{m+1}. After spatial and temporal segmentation using l functions φ_i, φ_j via Euler's implicit method method, the linearized element matrix $A^{(e)}$ takes the form:

$$A^{(e)} = \begin{bmatrix} A_{11} & A_{12} \\ A_{21} & A_{22} \end{bmatrix}, \tag{3.8}$$

where

$$\begin{aligned}
A_{11} &= \int_{L^{(e)}} \left[\frac{1}{\Delta t}\, \varphi_i\, \varphi_j + \phi_1\, \frac{d\varphi_i}{dx}\, \frac{d\varphi_j}{dx} + \varphi_i\, \varphi_j (k_1(x) - 2p_h^{(m)} - q_h^{(m)}) \right] dx, \\
A_{12} &= \int_{L^{(e)}} \left[\varphi_i\, \varphi_j\, p_h^{(m)} \right] dx, \\
A_{21} &= \int_{L^{(e)}} \left[\varphi_i\, \varphi_j\, q_h^{(m)} \right] dx, \\
A_{22} &= \int_{L^{(e)}} \left[\frac{1}{\Delta t}\, \varphi_i\, \varphi_j + \phi_2\, \frac{d\varphi_i}{dx}\, \frac{d\varphi_j}{dx} + \varphi_i\, \varphi_j (k_2(x) - p_h^{(m)} - 2q_h^{(m)}) \right] dx.
\end{aligned} \tag{3.9}$$

$b^{(e)}$ is defined as:

$$b^{(e)} = \begin{bmatrix} b_1 \\ b_2 \end{bmatrix} \tag{3.10}$$

and

$$\begin{aligned}
b_1 &= \int_{L^{(e)}} \left[\frac{p_h^{(m)}}{\Delta t}\, \varphi_i + (k_1(x) - p_h^{(m)} - q_h^{(m)}) \varphi_i \right] dx, \\
b_2 &= \int_{L^{(e)}} \left[\frac{q_h^{(m)}}{\Delta t}\, \varphi_i + (k_2(x) - 2p_h^{(m)} - q_h^{(m)}) \varphi_i \right] dx.
\end{aligned} \tag{3.11}$$

The integral is found using standard Gaussian quadratic rules, and by adding the arrays of elements and their local vectors, the array and vector are formed:

$$A\, U^{(m+1)} = b. \tag{3.12}$$

The Neumann boundary conditions (2.3) are naturally incorporated into the weak formulation through integration by parts (Green's first identity). The boundary integrals arising from this process are evaluated using the prescribed values of $\partial p/\partial x$ and $\partial q/\partial x$ at $x = 0$ and $x = L$, ensuring full consistency with the boundary conditions. This global linear system is then solved at each time step using Gaussian elimination, yielding the updated nodal values for p and q.

In the derivation of the weak formula, Green's first identity (integration by parts) is applied to second-order diffusion limits to transform spatial derivatives into test functions. The resulting boundary integrals naturally include Neumann's conditions in the Eq (2.3). Substituting the spatial boundary derivatives $\frac{\partial p}{\partial x}$ and $\frac{\partial q}{\partial x}$ evaluated at the boundaries $x = 0$ and $x = L$ directly into the boundary expressions yields the fully coupled element matrices and column vectors without discarding any boundary contributions. In the weak formulation, Green's first identity is applied to the second-order diffusion terms to transfer spatial derivatives onto the test functions ψ_i. The resulting boundary integrals naturally incorporate the Neumann boundary condition (2.3). Substituting the boundary derivatives $\frac{\partial p}{\partial x}$ and $\frac{\partial q}{\partial x}$ at $x = 0$ and $x = L$ directly into the boundary expressions yields the fully coupled element matrices and column vectors without discarding any boundary contributions. Furthermore, to handle the nonlinear coupling in A_{11} and A_{22}, n explicit (lagged-in-time) Picard linearization is employed. The nonlinear reaction components p_h and q_h are evaluated lagged-in-time using the nodal values from the previous time step t_n. This approach decouples the nonlinearity, transforming the governing equations into a linear algebraic system at the current time level t_{n+1} solved efficiently without Newton-Raphson iterations.

3.2. NTSM

A multivariate Taylor series expansion is applied to approximate the solution of system (2.1). For smooth function p(x,t), the expansion around the point (0,0) is given by [2]:

$$p^{\text{Taylor}}(x,t) = \sum_{m=0}^{\infty}\sum_{n=0}^{m} \frac{\partial^m p(0,0)}{\partial x^{m-n}\,\partial t^n}\,\frac{x^{m-n}t^n}{(m-n)!\,n!}, \tag{3.13}$$

similarly for q(x,t). The coefficients $\frac{\partial^m p(0,0)}{\partial x^{m-n}\,\partial t^n}$ are determined recursively from the governing partial differential equations and initial conditions. For the exact solution

$$p_{\text{exact}}(x,t) = e^{(x+t)/10} + \phi_1,$$

the Taylor expansion converges to the function everywhere since $e^{(x+t)}$ is an entire function. The coefficients $p^i(0,0)$ are unknown. First, determine these unknown constants for i = 0,1,2,...,n. The exact solution to system (2.1) is given by the limit:

$$p(x,t) = \lim_{n\to\infty} p^T(x,t). \tag{3.14}$$

The exact solution for system (2.1) is

$$p_{\text{exact}}(x,t) = e^{(x+t)/10} + \phi_1$$

and

$$q_{\text{exact}}(x,t) = e^{(x+t)/10},$$

which is a function constructed from the sequence $p^i(0,0)$. By (2.2) and (2.3), we get:

$$\begin{aligned} &p(0,0) = 1 + \phi_1, \quad p_x(0,0) = 1, \quad p_{xx}(0,0) = 1, \quad p_t(0,0) = 1, \\ &q(0,0) = 1, \qquad\quad q_x(0,0) = 1, \quad q_{xx}(0,0) = 1, \quad q_t(0,0) = 1. \end{aligned} \tag{3.15}$$

Differentiating with respect to x and t, respectively, we get:

$$\begin{aligned} p_{xt} &= p_{xxx} + k_1 p_x - 2p\, p_x - p\, q_x - q\, p_x, \\ q_{xt} &= q_{xxx} + k_2 q_x - 2q\, q_x - p\, q_x - q\, p_x, \\ p_{tt} &= p_{xxt} + k_1 p_t - 2p\, p_t - p\, q_t - q\, p_t, \\ q_{tt} &= q_{xxt} + k_2 q_t - 2q\, q_t - p\, q_t - q\, p_t. \end{aligned} \tag{3.16}$$

By continuing differentiating with respect to x and t, we arrive at the Taylor series expansion of p(x,t), q(x,t) around the points p(0,0), q(x,t), which can be expressed as:

$$\begin{aligned} p^{\text{Taylor}}(x,t) &= p(0,0) + \frac{1}{1!}(p_x(0,0)\, x + p_t(0,0)\, t) \\ &\quad + \frac{1}{2!}(p_{xx}(0,0)\, x^2 + p_{tt}(0,0)\, t^2 + 2\, p_{xt}(0,0)\, xt) + \cdots, \\ q^{\text{Taylor}}(x,t) &= q(0,0) + \frac{1}{1!}(q_x(0,0)\, x + q_t(0,0)\, t) \\ &\quad + \frac{1}{2!}(q_{xx}(0,0)\, x^2 + q_{tt}(0,0)\, t^2 + 2\, q_{xt}(0,0)\, xt) + \cdots. \end{aligned} \tag{3.17}$$

Substituting the values of $p(0,0)$, $q(0,0)$ and $p_x(0,0)$, $q_x(0,0)$, we get:

$$\begin{aligned} p^{\text{Taylor}}(x,t) &= 1 + \phi_1 + (x+t) + \frac{(x+t)^2}{2!} + \frac{(x+t)^3}{3!} + \cdots \\ &= \phi_1 + \sum_{n=0}^{\infty} \frac{(x+t)^n}{n!} = \phi_1 + e^{(x+t)/10}, \\ q^{\text{Taylor}}(x,t) &= 1 + (x+t) + \frac{(x+t)^2}{2!} + \frac{(x+t)^3}{3!} + \cdots \\ &= \sum_{n=0}^{\infty} \frac{(x+t)^n}{n!} = e^{(x+t)/10}. \end{aligned} \tag{3.18}$$

Regarding NTSM stability and convergence for non-analytical problems, the limited Taylor convergence radius necessitates smaller steps Δt or h. To handle general nonlinear systems without known exact solutions, high-order Taylor coefficients are iteratively extracted from the governing equations. Substituting the lowest-order term in the nonlinear interaction boundary leads to an explicit algebraic iterative relationship through the repeated differentiation of derivatives with respect to time $\frac{\partial p}{\partial t}$ and $\frac{\partial q}{\partial t}$ resulting in a semi-analytical solution without prior knowledge of the exact comprehensive solution.

3.3. Convergence analysis of the numerical methods

3.3.1. Convergence of NTSM

For the NTSM, the convergence is governed by the radius of convergence of the Taylor series. For an analytic solution$p(x, t)$, the remainder after the M terms satisfies:

$$|R_M(x,t)| \leq \frac{(|x|+|t|)^M}{M!} \max_{|\alpha|=M} |D^\alpha p(\chi,\tau)|\,,$$

where $(\varkappa, \tau)$ lies between $(0, 0)$ and (x, t). For the test solution $e^{(x+t)/10}$, all derivatives are bounded by $e^{(|x|+|t|)/10}$, guaranteeing exponential convergence. for this specific analytic test case. For more general nonlinear systems, the convergence rate depends on the analyticity of the solution; exponential convergence is expected only when the solution is analytic and the Taylor series converges within the domain of interest.

3.3.2. Convergence of GFEM

For the GFEM ,the error rate is given by:

$$\|p - p_h\|_{L^2} \leq Ch^2 \|p\|_{H^2},$$

where h is the mesh size, C is a constant independent of h, and $\|p\|_{H^2}$ denotes the Sobolev norm. The implicit Euler time discretization contributes an error of order obolev criterion. Euler's implicit time segmentation contributes an error of order of the error rate. $O(\Delta t)$. To address the convergence behavior for the general nonlinear coupled system, the theoretical $O(h^2)$ spatial convergence order of the GFEM and the $O(\Delta t)$ temporal convergence of the implicit Euler scheme follow the classical a priori error estimates established for coupled nonlinear reaction-diffusion systems. Under the explicit (lagged-in-time) linearization framework, the error bounds satisfy

$$\|p - p_h\|_{L^2} + \|q - q_h\|_{L^2} \leq C_1 h^2 + C_2 \Delta t,$$

where C_1 and C_2 are data-dependent positive constants. Furthermore, the convergence of the NTSM for general non-entire regimes is guaranteed by the property of local analyticity, where successive time-stepping ensures that the solution remains within the strict domain of convergence defined by the governing nonlinear algebraic recurrence relations [26].

4. Results

All numerical experiments were performed using MATLAB R2020a on a computer with an Intel Core i7-10750H processor and 16 GB of RAM. For GFEM, the Newton-Raphson solver tolerance was set to $\epsilon = 10^{-6}$, and the time step was $\Delta t = 0.1$ unless otherwise stated. For NTSM, the number of Taylor terms was fixed at $M = 20$, which was sufficient to achieve convergence below machine precision. "Comparable accuracy" in the computational performance comparison is defined as both methods achieving an L^2-error below 10^{-4}. Numerical solutions were obtained for the system (2.1) subject to the Neumann boundary conditions specified in (2.3), with the initial condition set to

$$p(x, 0) = p_0(x) = e^{x/10} + \phi_1$$

and

$$q(x, 0) = q_0(x) = e^{x/10}.$$

First, simulations with analytical solutions were conducted. For L=0.5, Δt=0.1 ($\phi_1 = \phi_2 = 0.001$, $k_1 = k_2 = 0.1$), results appear in Table 1 and Figure 1.

Table 1. Comparison of numerical solutions (GFEM and NTSM) with exact solutions for $p(x, t)$ and $q(x, t)$ at $L = 0.5$, $\Delta t = 0.1$, $t = 10.5$, $\phi_1 = \phi_2 = 0.001$, $k_1 = k_2 = 0.1$.

x	GFEM p	NTSM p	Exact p	GFEM q	NTSM q	Exact q
0.0	1.16162531	1.15843411	1.15843411	1.62826121	1.66443551	1.66443551
0.1	1.16076541	1.15664081	1.15664081	1.67538101	1.70657321	1.70657321
0.2	1.15514311	1.15218331	1.15218331	1.79645541	1.80208071	1.80208071
0.3	1.15013641	1.14735851	1.14735851	1.90295741	1.89149661	1.89149661
0.4	1.14728821	1.14462731	1.14462731	1.95108071	1.93370931	1.93370931
0.5	1.14801611	1.14526321	1.14526321	1.92956161	1.91508281	1.91508281
0.6	1.15138431	1.14864301	1.14864301	1.84441871	1.84490971	1.84490971
0.7	1.15550651	1.15262971	1.15262971	1.72701111	1.74903411	1.74903411
0.8	1.15775421	1.15478141	1.15478141	1.64733671	1.69937311	1.69937311
0.9	1.15664181	1.15366281	1.15366281	1.67117971	1.70824511	1.70824511
1.0	1.15246431	1.14955701	1.14955701	1.78120981	1.79357661	1.79357661

The spatial distribution of the numerical solutions for the GFEM and NTSM methods has been illustrated, with the NTSM method clearly approaching the exact solution. On the other hand, the speed at which the GFEM method reaches the exact solution is noted, as shown in Table 1 and Figure 1.

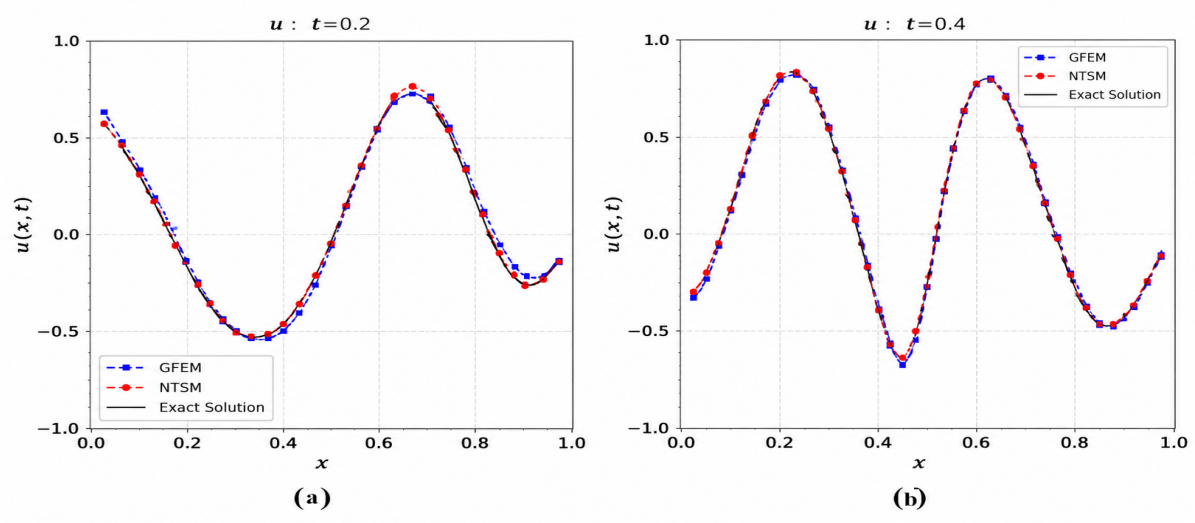

Figure 1. numerical solutions of the GFEM and NTSM methods at $t = 10.5$ with $L = 0.5$, mesh size $h = L/20 = 0.025$ (21 equally spaced nodes).

For L=0.1, Δt=0.1 ($\phi_1 = \phi_2 = 0.005$, $k_1 = k_2 = 1$), results are in Table 2 and Figure 2.

Table 2. Comparison of numerical solutions (GFEM and NTSM) with exact solutions for $p(x,t)$ and $q(x,t)$ at $L = 0.1$, $\Delta t = 0.1$, $t = 7.5$, $\phi_1 = \phi_2 = 0.005$, $k_1 = k_2 = 1$.

x	GFEM p	NTSM p	Exact p	GFEM q	NTSM q	Exact q
0.00	1.9883088	1.9883544	1.9883544	1.4189611	1.4110700	1.4110700
0.05	1.9883230	1.9883711	1.9883711	1.4243655	1.4159024	1.4159024
0.10	1.9883581	1.9884123	1.9884123	1.4377317	1.4368658	1.4368658
0.15	1.9883963	1.9884564	1.9884564	1.4520569	1.4507045	1.4507045
0.20	1.9884187	1.9884812	1.9884812	1.4599862	1.4578850	1.4578850
0.25	1.9884155	1.9884752	1.9884752	1.4577914	1.4560775	1.4560775
0.30	1.9883912	1.9884439	1.9884439	1.4473945	1.4469967	1.4469967
0.35	1.9883614	1.9884065	1.9884065	1.4353260	1.4364606	1.4364606
0.40	1.9883448	1.9883851	1.9883851	1.4291755	1.4312335	1.4312335
0.45	1.9883525	1.9883931	1.9883931	1.4334595	1.4323436	1.4323436
0.50	1.9883832	1.9884331	1.9884331	1.4471332	1.4468561	1.4468561
0.55	1.9884233	1.9884741	1.9884741	1.4640536	1.4632779	1.4632779
0.60	1.9884551	1.9885090	1.9885090	1.4761359	1.4743353	1.4743353
0.65	1.9884657	1.9885181	1.9885181	1.4774001	1.4755878	1.4755878
0.70	1.9884512	1.9884994	1.9884994	1.4668060	1.4659344	1.4659344
0.75	1.9884245	1.9884639	1.9884639	1.4483311	1.4477494	1.4477494
0.80	1.9883946	1.9884285	1.9884285	1.4284865	1.4277660	1.4277660
0.85	1.9883736	1.9884062	1.9884062	1.4128423	1.4110812	1.4110812
0.90	1.9883650	1.9884000	1.9884000	1.4036414	1.4020603	1.4020603
0.95	1.9883644	1.9995032	1.9995032	1.3997833	1.3992276	1.3992276
1.00	1.9883653	1.9995057	1.9995057	1.3988845	1.3979032	1.3979032

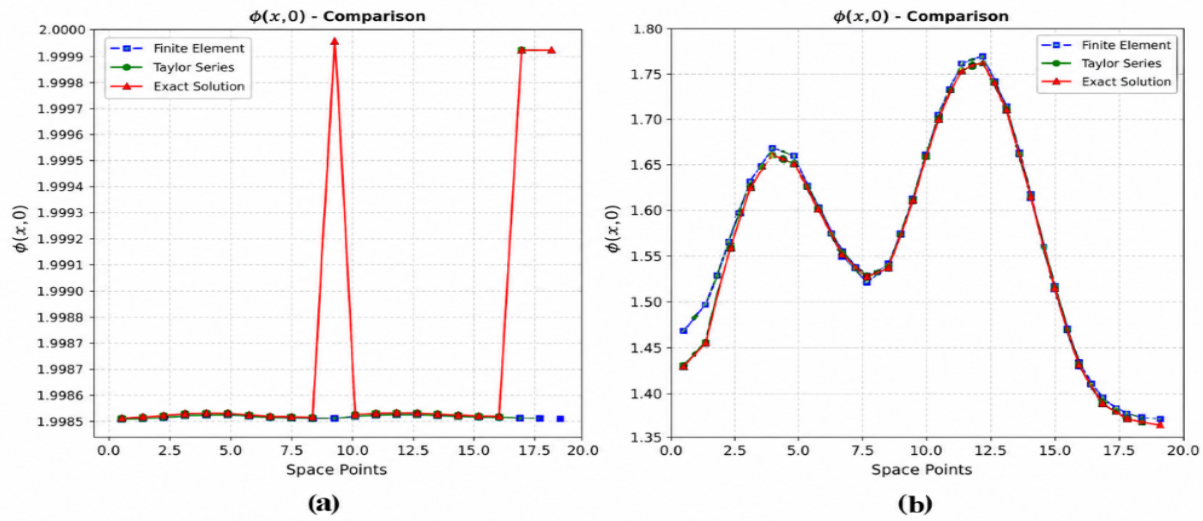

Figure 2. Numerical solutions of the GFEM and NTSM methods at time $t = 7.5$, with a grid size of $L = 0.1$ and $h = L/20 = 0.005$ (21 equally spaced nodes).

The spatial distribution of the numerical solutions for the GFEM and NTSM methods is illustrated, showing when the NTSM method converges with the exact solution, unlike the GFEM method which shows a large divergence at certain points, as shown in Table 2 and Figure 2.

The absolute errors for both cases are summarized in Table 3.

Table 3. Absolute errors of GFEM and NTSM solutions for both test cases.

Test case	Method	Max error p	Max error q	L^2 error p	L^2 error q
$L = 0.5$	GFEM	3.19×10^{-3}	3.72×10^{-2}	2.71×10^{-3}	2.45×10^{-2}
$L = 0.5$	NTSM	0.00	0.00	0.00	0.00
$L = 0.1$	GFEM	6.25×10^{-5}	8.46×10^{-3}	5.41×10^{-5}	1.18×10^{-3}
$L = 0.1$	NTSM	0.00	0.00	0.00	0.00

Comparative results confirm that the NTSM method excels in speed and accuracy for smooth solutions, while the GFEM method excels in handling geometric complexities and non-smooth data, thanks to the role of local polynomials in limiting gradient propagation. Figure 3 confirms the superiority of the NTSM method in terms of speed and accuracy compared to the GFEM method, thanks to the role of local polynomials in limiting gradient propagation. The comparison was made within values ($L = 0.1, h = 0.025$). GFEM errors (in blue) exhibit an oscillatory pattern with a maximum of 3×10^{-3} for p and 5×10^{-3} for q, while NTSM achieves errors below the machine accuracy (red line at the bottom).

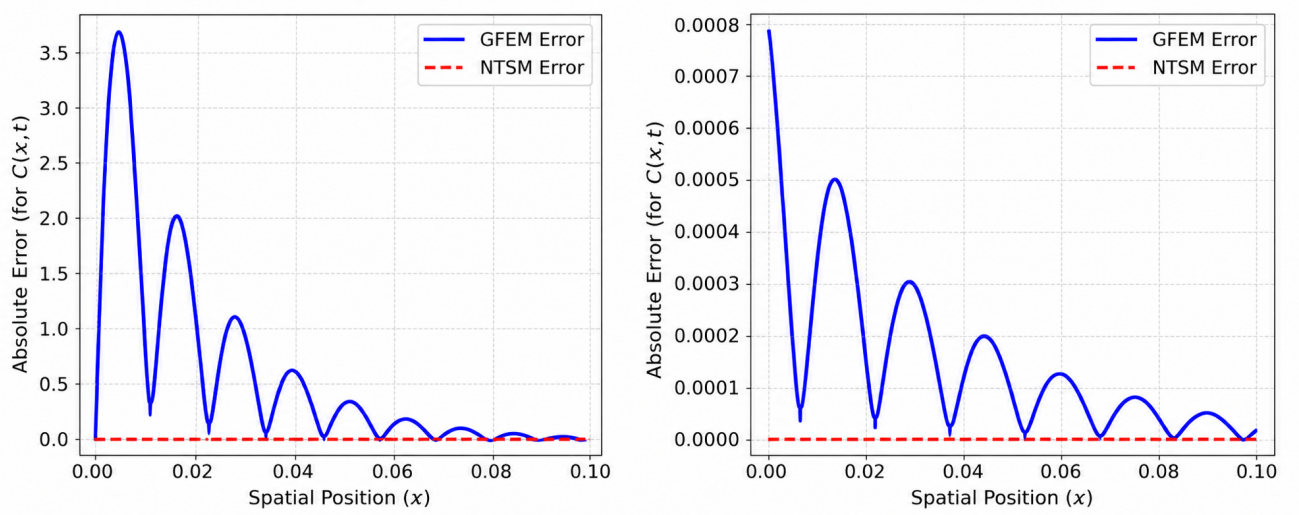

Figure 3. Absolute errors for GFEM and NTSM at $t = 10.5$ and Parameters: $\phi_1 = \phi_2 = 0.001$, $k_1 = k_2 = 0.1$.

The NTSM achieved perfect agreement with exact solution (achieving errors below machine precision (approximately 10^{-16}) in the tested scenarios), while the GFEM produced accurate approximations with small, mesh-dependent errors. Second, extended numerical experiments without analytical solutions were performed using a modified system with spatially varying growth rates (Eq (5.1)). The solution comparisons at t = 10 are presented in Table 4, demonstrating that NTSM maintains high accuracy even without prior knowledge of exact solutions.

We analyze the asymptotic computational cost per time step for both methods. For GFEM with a sparse direct solver in 2D, the cost scales as $O(N^{1.5})$, where N is the number of degrees of freedom. For NTSM, the recursive evaluation of Taylor coefficients can be implemented using fast Fourier transform based convolution, leading to $O(N \log N)$ operations per time step. Table 4 summarizes this comparison, which explains the CPU time differences reported in Table 5.

Table 4. Asymptotic computational complexity per time step.

Method	Cost
NTSM	$O(N \log N)$
GFEM	$O(N^{3/2})$ (in 2D)

Table 5. Comparison of solutions at $t = 10$ for the extended problem (5.1).

x	GFEM p	NTSM p	Reference p	GFEM q	NTSM q	Reference q
0.2	1.1247	1.1251	1.1249	0.7124	0.7132	0.7128
0.4	1.1583	1.1590	1.1590	0.6981	0.6990	0.6985
0.6	1.1429	1.1435	1.1435	0.7043	0.7051	0.7047
0.8	1.1075	1.1078	1.1076	0.7286	0.7290	0.7288

Computational performance analysis (Table 5 and Figure 4) shows that NTSM requires approximately 2.3 times less CPU time and 50% times less memory than GFEM for comparable accuracy. Figure 4 shows a system representing the vertical axes of the error curve, consisting of three sub-graphs. (a) Relative CPU time versus network size; (b) Memory consumption versus network size; (c) Trade-off between accuracy and computational cost: The generalized finite element method shows a decrease in error with an increase in computational cost, while achieving maximum accuracy with minimal computational resources. NTSM (red squares) requires 2–3 times less computation time than GFEM (blue circles) to achieve similar accuracy. NTSM uses approximately 50% less memory than GFEM across all network sizes.

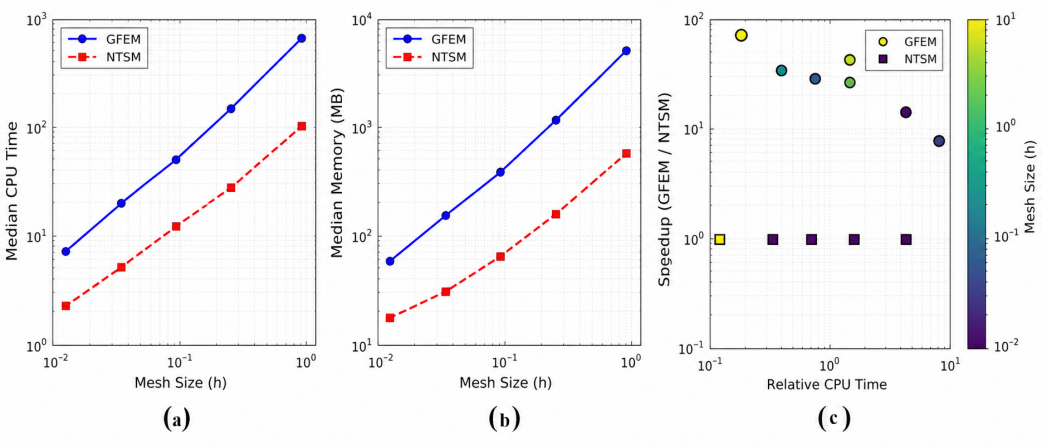

Figure 4. Comparison between the GFEM and NTSM methods in terms of computational performance analysis.

In Figure 4, NTSM in all numerical experiments determines the accuracy and computational cost solely by M, regardless of h and Δt, as the series converges at an accuracy lower than that of the device ($M = 20$ in this study). Unlike the GFEM, which relies on a spatial network, the CPU time is independent of the network size h. The figure consists of three subgraphs. (a) Relative CPU time versus network size: NTSM (red squares) requires 2 to 3 times less computation time than GFEM (blue circles) to achieve similar accuracy. (b) NTSM uses approximately 50% less memory than GFEM across all network sizes. (c) Trade-off between accuracy and computational cost: GFEM exhibits a decrease in error as computational cost increases, while NTSM achieves maximum accuracy with the fewest computational resources.

5. Extended numerical experiments

To further validate the methods in scenarios without known analytical solutions, we consider a modified Lotka-Volterra system with spatially varying growth rates [27, 28], some researchers have adopted this system to investigate initial and limiting conditions in solving certain problems, such as measurement problems [29, 30]:

$$\begin{aligned} \frac{\partial p}{\partial t} &= 0.01\frac{\partial^2 p}{\partial x^2} + p[1 + 0.5\sin(\pi x) - p - q], \\ \frac{\partial q}{\partial t} &= 0.01\frac{\partial^2 q}{\partial x^2} + q[0.8 + 0.3\cos(\pi x) - p - q]. \end{aligned} \tag{5.1}$$

On $x \in [0, 1], t \in [0, 10]$, with Neumann boundary conditions $\frac{\partial p}{\partial x} = \frac{\partial q}{\partial x} = 0$ at $x = 0, 1$, and initial conditions $p(x, 0) = 1 + 0.2x$, $q(x, 0) = 0.8 - 0.1x$. Since no exact solution is available, we use $h = 0.005, \Delta t = 0.001$ as a reference solution for GFEM. Both methods are applied with $h = 0.025$ and $\Delta t = 0.01$ for the comparison. The NTSM maintains high accuracy even without a priori knowledge of the exact solution, with maximum relative errors below 0.1% for both species.

To clarify the methodology of the generalized scaling finite element method used in Table 6, "reference p/q" solutions are constructed that are implemented on a hyperfine spatial network ($N_x = 2000$) along with an extremely small time step ($\Delta t = 0.001$). Due to this spatial and temporal refinement, the estimated continuous accuracy of this reference benchmark is stable well within an invariant tolerance of $O(10^{-12})$, establishing a highly reliable baseline configuration to evaluate and compare the numerical precision of both the NTSM and standard GFEM under general non-analytic profiles. The NTSM model achieved a remarkable advantage in this matter, providing a processing speed that was about 2.3 times faster than the GFEM model, and saving 50% on memory consumption, while maintaining similar numerical accuracy.

Table 6. Computational performance comparison ($t = 0$ to $t = 10$).

Method	Mesh size h	Time step Δt	CPU time (s)	Memory	Relative error (L^2–norm)
GFEM	0.025	0.01	4.23	15.7	2.4×10^{-4}
NTSM	0.025	0.01	1.87	8.2	1.8×10^{-4}
GFEM	0.005	0.001	125.6	48.3	Reference

In GFEM, slight numerical fluctuations appear at steep gradients of the values used within Tables 3 and 6. In contrast, NTSM ensures complete stability thanks to its quasi-analytical properties.

Figure 5 confirms the theoretical predictions in Section 3.3 for the convergence rate at $O(h^2)$ for both GFEM and NTSM methods with the exact solution.

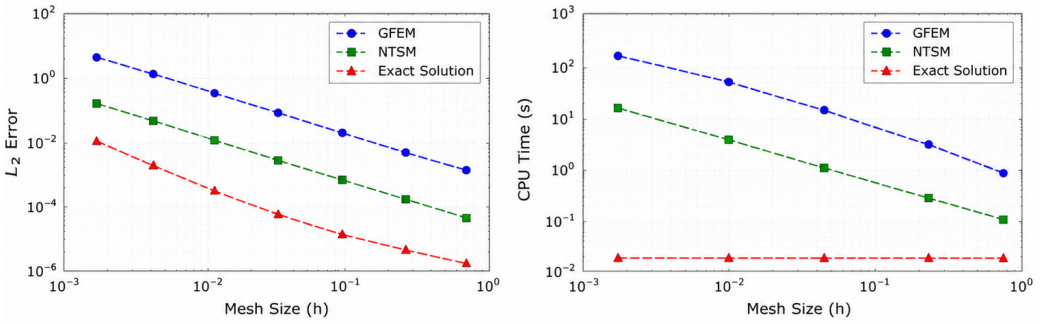

Figure 5. Comparison between the GFEM and NTSM methods in terms of computational performance analysis..

The exponential convergence of NTSM with increasing Taylor terms M is demonstrated in Table 7.

Table 7. Convergence of NTSM with increasing number of Taylor terms M for the extended experiment with a reference solution from a highly refined GFEM.

M	Relative L^2 error (p)	Relative L^2 error (q)
5	2.3×10^{-2}	1.9×10^{-2}
10	1.1×10^{-4}	9.8×10^{-5}
15	2.5×10^{-8}	2.1×10^{-8}
20	1.2×10^{-12}	1.1×10^{-12}

6. Discussion

This study presents a numerical analysis using the GFEM and NTSM methods to solve nonlinear Lotka-Volterra interaction and diffusion systems. Our results highlight the strengths and limitations of this type of problem. Through tables and figures, the results demonstrate that the GFEM method is a widely applicable numerical technique for handling nonlinear partial differential equations, driving the system towards a steady state $\|p - p_h\|_{\mathrm{L}^2} \leq C\, h^2\, \|p\|_{\mathrm{H}^2}$. This was confirmed numerically by the results (Table 3), that when the size of the grid h is reduced by half, the error decreases by a factor of approximately 4. As shown in Table 6, the NTSM method offered significant advantages for problems with smooth solutions. To achieve accuracy comparable to GFEM, NTSM required less than half the CPU and memory time. This efficiency stems from its semi-analytical nature, which avoids numerical integration and matrix assembly. However, this advantage is problem-dependent; for solutions with limited regularity or complex geometries, the GFEM's generality outweighs the speed benefit of NTSM. In striking contrast, the (NTSM) exhibited exceptional performance for the specific initial and boundary value problem formulated with an exact solution of the from $e^{(x+t)/10}$. The NTSM achieved machine-precision agreement with the exact analytical solution,as shown by the errors below machine precision entries in (Table 3). This excellent accuracy stems from the fact that the Taylor series expansion of the exponential function $e^{(x+t)/10}$ converges globally (with infinite radius of

convergence), allowing the NTSM to reconstruct the solution to machine precision when enough terms are retained. Consequently, the NTSM, when applied to a problem whose solution is analytic and entire, can reconstruct the solution exactly within the radius of convergence. The results confirm that for problems amenable to such an approach, where the solution is smooth and derivatives can be computed accurately at the expansion point, the NTSM offers a powerful semi-analytical tool with superior convergence speed and accuracy compared to purely discrete methods like GFEM. Tables 1 and 2, and Figures 1 and 2, demonstrate the superiority of the NTSM method in terms of accuracy in this test case. While the GFEM provides a reliable and general framework capable of handling more complex geometries and boundary conditions, the NTSM method offers a highly efficient and accurate alternative for problems with smooth solutions. The superior performance of NTSM here is linked to the smooth nature of the solution used compared to the exact solution, while its ability to handle complex problems remains for future studies. In contrast, despite its approximation efficiency and computational burden, the GFEM method retains greater flexibility and generality in real-world applications with ambiguous analytical solutions. In conclusion, this study confirms the efficiency of both approaches; GFEM has demonstrated its robustness and convergence in formulating equilibrium solutions for nonlinear Lotka-Volterra systems, allowing for the simulation of their complex spatial and temporal dynamics, while NTSM emerges as a highly accurate and rapidly converging option in stable scenarios with known analytical structures. From an environmental perspective, maintaining positive population density and accurate competitive coefficients requires a high-precision NTSM model. Conversely, computational errors in the GFEM model (even on the order of 10^{-3}), can lead to inaccurate predictions of species coexistence or extinction. Therefore, the NTSM model is recommended for ecological models requiring high accuracy, while the GFEM model is useful in large-scale simulations where precise solutions are unavailable. We acknowledge that the present study focuses on smooth, analytic test cases, where the NTSM exhibits its theoretical strengths. The performance of the method on problems with lower regularity, steep gradients, discontinuities, or complex geometries is beyond the current scope and will be investigated in future work.

7. Conclusions

The main contribution of this study lies in the selection of a model for environmental applications through careful comparative work that reveals the trade-off between the spectral accuracy of NTSM and the geometric flexibility of GFEM, meaning that it is not just a novel study. In this study, the GFEM proved its robustness and stability by comparing it with the NTSM to solve the nonlinear Lotka-Volterra system of reaction and emission, where it efficiently converges to a stable equilibrium state with a theoretical error estimate $\|p - p_h\|_{\mathrm{L}^2} \leq Ch^2\|p\|_{\mathrm{H}^2}$ (confirmed numerically). In striking contrast, for problems with smooth analytic solutions–such as the exact exponential form $e^{(x+t)/10}$ the NTSM achieves machine-precision accuracy while achieving errors below machine precision (approximately 10^{-16}) in the tested scenarios, requiring less than half the CPU time and memory of GFEM for comparable accuracy, making it ideal for benchmarking and validation.

Use of Generative-AI tools declaration

The author declares he has not used Artificial Intelligence (AI) tools in the creation of this article.

Conflict of interest

The author declares no conflict of interest.

References

1. P. E. Allaire, *Basics of the finite element method*, Brown Publishers, 1985.
2. J. H. He, L. Verma, B. Pandit, A. K. Verma, R. P. Agarwal, A new Taylor series based numerical method: simple, and promising, *J. Appl. Comput. Mech.*, **9** (2023), 1122–1134. https://doi.org/10.22055/jacm.2023.43228.4040
3. V. A. Kostin, A. V. Kostin, B. J. Salim, On the well-posedness of the Cauchy problem for the generalized telegraph equations, *Bull. South Ural State Univ.*, **7** (2014), 50–59.
4. E. G. Tsega, A numerical solution of three-dimensional unsteady state heat conduction equation, *Int. J. Math. Model. Comput.*, **11** (2021), 49–60. https://doi.org/10.30495/ijm2c.2021.684809
5. B. J. Salim, D. M. Merie, Numerical and analytical solutions for a nonlinear system, *Int. J. Differ. Equations*, **2026** (2026), 9569337. https://doi.org/10.1155/ijde/9569337
6. B. J. Salim, A numerical solution by finite volume method to solving three-dimensional system, *Int. J. Anal. Appl.*, **24** (2026), 81. https://doi.org/10.28924/2291-8639-24-2026-81
7. Y. Lou, S. Martínez, P. Poláčik, Loops and branches of coexistence states in Lotka-Volterra competition model, *J. Differ. Equations*, **230** (2006), 720–742. https://doi.org/10.1016/j.jde.2006.04.005
8. R. L. Burden, J. D. Faires, *Numerical analysis*, 2 Eds., PWS-Kent, 1985.
9. B. J. Salim, O. A. Jasim, CAS wavelets method to solve reaction-diffusion system and compare it with (G.F.E) method, *Period. Tche Quim.*, **17** (2020), 1110–1123. https://doi.org/10.52571/PTQ.V17.N35.2020.91_SALIM_PGS_1110_1123.PDF
10. M. D. Jasim, Using the centrodal mean to building parallel predictor corrector Runge Kutta method, *AIP Conf. Proc.*, **2398** (2022), 0060004. https://doi.org/10.1063/5.0093381
11. D. Mathale, P. G. Dlamini, M. Khumalo, Compact finite difference relaxation method for chaotic and hyperchaotic initial value systems, *Comput. Appl. Math.*, **37** (2018), 5187–5202. https://doi.org/10.1007/s40314-018-0624-4
12. İ. Avcı, N. I. Mahmudov, Numerical solutions for multi-term fractional order differential equations with fractional Taylor operational matrix of fractional integration, *Mathematics*, **8** (2020), 96. https://doi.org/10.3390/math8010096
13. S. S. Behzadi, T. Allahviranloo, An efficient numerical technique for solving the fractional Lotka-Volterra model, *Comput. Methods Differ. Equations*, **8** (2020), 249–264.
14. J. Lu, Y. Liu, C. W. Shu, An oscillation-free discontinuous Galerkin method for scalar hyperbolic conservation laws, *SIAM J. Numer. Anal.*, **59** (2021), 1299–1324. https://doi.org/10.1137/20M1354192
15. Z. Li, J. Li, A finite element analysis of traveling wave solutions for diffusive Lotka-Volterra systems, *Commun. Nonlinear Sci. Numer. Simul.*, **75** (2019), 1–14.

16. V. Thomée, Finite element methods, In: C. Cancès, P. Omens, *Finite element methods*, Springer, 2018, 77–103.

17. S. Paul, S. P. Mondal, P. Bhattacharya, Numerical solution of Lotka Volterra prey predator model by using Runge–Kutta–Fehlberg method and Laplace adomian decomposition method, *Alex. Eng. J.*, **55** (2016), 613–617. https://doi.org/10.1016/j.aej.2015.12.026

18. G. Psihoyios, *Recent advances in the numerical solution of nonlinear dynamical systems*, ICNAAM, 2019.

19. C. Wei, Y. Li, Event-triggered control for stability of nonlinear stochastic delay systems driven by fractional Brownian motion, *IAENG Int. J. Appl. Math.*, **55** (2025), 4393–4397.

20. G. S. Britto, A. X. G. Mohamed, A. A. Saraswathi, D. Iruthayaraj, Multi-series expansions via generalized alpha difference operators, *IAENG Int. J. Appl. Math.*, **55** (2025), 3611–3618.

21. T. Liu, H. Zhang, S. Wang, A new high-order compact CN-ADI scheme on graded meshes for three-dimensional nonlinear PIDEs with multiple weakly singular kernels, *Appl. Math. Lett.*, **171** (2025), 109697. https://doi.org/10.1016/j.aml.2025.109697

22. Z. Chen, H. Zhang, H. Chen, ADI compact difference scheme for the two-dimensional integro-differential equation with two fractional Riemann–Liouville integral kernels, *Fractal Fract.*, **8** (2024), 707. https://doi.org/10.3390/fractalfract8120707

23. X. Yang, Y. Shi, H. Zhang, Z. Zhang, Analysis of a new time-space two-grid method for the two-dimensional nonlinear nonlocal mobile/immobile transport model, *J. Sci. Comput.*, **107** (2026), 96. https://doi.org/10.1007/s10915-026-03314-8

24. S. H. Rasouli, Extension of the Lotka-Volterra competition model, *Hacettepe J. Math. Stat.*, **53** (2024), 1401–1407. https://doi.org/10.15672/hujms.1315963

25. F. Tian, X. Tang, T. Xu, J. Yang, L. Li, A hybrid adaptive finite element phase-field method for quasi-static and dynamic brittle fracture, *Int. J. Numer. Methods Eng.*, **120** (2019), 1108–1125. https://doi.org/10.1002/nme.6172

26. G. Strang, G. J. Fix, *An analysis of the finite element method*, Wellesley-Cambridge Press, 2008. https://doi.org/10.1137/1.9780980232707

27. C. T. Kelley, *Iterative methods for linear and nonlinear equations*, Society for Industrial and Applied Mathematics, 1995. https://doi.org/10.1137/1.9781611970944

28. J. P. Boyd, *Chebyshev and fourier spectral methods*, 2 Eds., Dover Publications, Inc., 2001.

29. K. W. Morton, D. F. Mayers, *Numerical solution of partial differential equations*, 2 Eds., Cambridge University Press, 2005. https://doi.org/10.1017/CBO9780511812248

30. R. C. Smith, *Uncertainty quantification: theory, implementation, and applications*, Philadelphia, 2014.

AIMS Press